JOURNAL OF GEOPHYSICAL RESEARCH, VOL. 97, NO. D16, PAGES 18,173–18,183, NOVEMBER 20, 1992

Radiometric Determination of Water Vapor and Liquid Water and Its Validation With Other Techniques

R. PETER AND N. KÄMPFER

Institute of Applied Physics, University of Bern, Bern, Switzerland

For remote sensing applications in the field of atmospheric physics it is necessary to know the highly variable part of the tropospheric water vapor absorption. With a dual-channel microwave radiometer, operating at 21.3 and 31.5 GHz, the estimation of the water vapor and liquid water content is possible. The retrieval is performed iteratively with an algorithm using simplified model profiles of the troposphere and a millimeter wave absorption model. This site-independent profile algorithm changes a model atmosphere until the calculated and measured sky brightness temperatures do agree. Integrated precipitable water vapor (IWV) and integrated liquid water (ILW) are obtained by integrating over the corresponding profiles. By the use of the absorption model sky brightness temperatures, opacities or propagation delays at other frequencies up to 1000 GHz can be calculated. Simulations with a few thousand test profiles showed that the rms error, excluding that of the absorption model, is about 3% for the IWV and between 10% and 20% for the ILW (ILW > 0.1 mm), while for the predicted opacities at 90, 142, and 204 GHz the error ranges between 15% and 25%. The performance of the algorithm and the water vapor radiometer has been checked with independent brightness temperature measurements at 142 and 204 GHz, respectively, IR spectroscopic measurements and radiosonde data. The independent measurements showed all a good agreement with the retrieved quantities of the profile algorithm.

1. INTRODUCTION

The continuous observation of atmospheric water vapor and liquid water (clouds) is obviously important for meteorological purposes. Besides this, the effect of vapor and liquid phase water content on the spectral properties of the propagation of electromagnetic waves is of high relevance to communication and remote sensing applications.

In particular, tropospheric millimeter wave absorption and emission is an important factor in ground-based observations of millimeter wave spectra, which are to be used in retrievals of minor constituents (e.g., CLO and O^3) [*Kämpfer et al.*, 1991; *Gerber and Kämpfer*, 1991] and other parameters of the stratosphere.

Under nonprecipitating conditions, the spectral properties of the troposphere are mainly determined by the height distributions of temperature, pressure, oxygen, water vapor, and liquid water (clouds) [*Waters*, 1976; *Ulaby et al.*, 1981]. For the total water vapor and liquid water content above ground, the notion of the integrated precipitable water vapor (IWV) and the integrated liquid water (ILW) are commonly used in meteorology. Both quantities have a high temporal and spatial variability which makes it difficult to estimate them from surface humidity data. A ground-based 20/30 GHz radiometer can provide the necessary information for these atmospheric parameters [*Elgered et al.*, 1982; *Peter and Kämpfer*, 1991].

Usually, a linear retrieval algorithm whose coefficients are empirically tailored to the observing site with radiosonde measurements is used for the determination of IWV and ILW [*Westwater and Guiraud*, 1980].

In contrast to this approach, we use a profile algorithm including the absorption model of *Liebe* [1989] where a parameterized representation of water vapor $\rho(z)$ and liquid water $\rho_L(z)$ (including clouds) was adjusted until the calculated and measured brightness temperatures do agree. IWV and ILW are obtained in a second step by integrating $\rho(z)$ and $\rho_L(z)$. The profile retrieval algorithm has the advantage that it does not depend on the observing site and that each contribution of dry air, water vapor, and liquid water could be evaluated separately because we calculate the absorption coefficients corresponding to the measured situation. With the knowledge of the estimated water vapor and liquid water profiles from the water vapor radiometer (WVR) data, it is then possible to predict the sky brightness temperature, opacity, and the transmission at other frequencies as 142 GHz (ozone spectrum) or 204 GHz (ClO spectrum) for an arbitrary location and observing angle. This is a most useful application in ground-based radiometric observation of the atmosphere where only stratospheric emission is of interest and where the influence of the troposphere has to be corrected for.

At Bern (47N, 7.5E, 550 meters above sea level (masl)), where we have a typical mid-latitude climate, two different radiometers operating at 142 and 204 GHz were used in order to validate the retrieval algorithm and the absorption model. The results of this comparison will be discussed in section 7 of this paper.

During a period of 6 months, continuous measurements have been carried out in the Swiss Alps at the "Hochalpine Forschungsstation Jungfraujoch." Since this station is 3580 m above sea level, it is considered to be a very dry site and therefore ideal for astronomical or atmospheric observations. The quantitative verification and the need for water vapor statistics for the users of the station were two reasons to install the radiometer there.

Other reasons were the possibility to compare our retrieved IWV with those of an IR spectrometer at the same place and the test of operational characteristics of our radiometer in an extremely dry atmosphere.

Paper number 92JD01717.
0148-0227/92/92JD-01717$05.00

2. PROFILE ALGORITHM AND MODELING

The sensitivity of the integrated quantities IWV and ILW with respect to altitude variations of the water distribution is lowest for a frequency pair around 20 and 30 GHz, when using the concept of linearized brightness temperatures and the corresponding linear retrieval [*Wu*, 1979]. As a result the optimum frequencies for an alpine climate are found to be 21.3 and 31.5 GHz [*Elgered et al.*, 1985]. They might change slightly for different climatological situations because they are chosen in such a way that the profile dependence of the linear algorithm for a given site is minimized.

Our algorithm does not use coefficients tailored to local climatology at the optimum frequencies, therefore a small deviation from these frequencies is not critical, since our nonlinear algorithm takes into account the profile dependence by using reasonable altitude distributions of temperature, water vapor, and liquid water. In spite of this fact, it is better to use a frequency pair close to the optimum one in order to minimize uncertainties in the line shape and line width parameters of the 22.235-GHz H_2O transition.

The optical thickness of an atmospheric layer from ground (z_0) to an altitude z for a frequency ν is given by

$$\tau(z, \nu) = \int_{z_0}^{z} \alpha(z, \nu)\, dz \tag{1}$$

where $\alpha(z, \nu)$ is the absorption coefficient (nonscattering case) dependent on temperature, pressure, oxygen, water vapor, and liquid water which can be calculated with an absorption model [e.g., *Liebe*, 1989].

The measured radiation for an upward looking radiometer expressed in terms of brightness temperature is given by the radiative transfer equation [*Waters*, 1976]

$$T_B(\nu) = T_C e^{-\tau(\infty,\nu)} + \int_0^{\infty} T(z)\alpha(z,\nu)e^{-\tau(z,\nu)}\, dz \tag{2}$$

where T_C is the cosmic background radiation of 2.64 K [*De Amici et al.*, 1991] and $T(z)$ is the temperature profile of the atmosphere.

Our profile algorithm makes no attempt to relate linearly the measured brightness temperatures $T_{B,\mathrm{Meas}}$ to the IWV or ILW. In our case the brightness temperatures T_B for a given model atmosphere are calculated according to (2) and compared with $T_{B,\mathrm{Meas}}$. Appropriate model atmosphere parameters are then changed in order to minimize the differences of T_B and $T_{B,\mathrm{Meas}}$ for both frequencies.

For the calculation of the absorption coefficients $\alpha(z, \nu)$ the updated version of the millimeter wave propagation model (MPM) [*Liebe*, 1985, 1989] is used. The most recent version contains a improved formulation for the permittivity of liquid water [*Liebe et al.*, 1991] and a new set of oxygen overlapping coefficients at 60 GHz [*Liebe et al.*, 1992]. Input parameters for MPM are barometric pressure, temperature, relative humidity, suspended droplet concentration, and rainfall rate. The total absorption coefficient consists of several additive terms

$$\alpha(z,\nu) = \alpha_L + \alpha_C + \alpha_D + \alpha_R \tag{3}$$

where α_L is the contribution of all relevant H_2O and O_2 lines up to 1000 GHz, α_C is the continuum absorption (empirical) due to far-wing contribution of strong H_2O lines above 1000 GHz and contributions of nonresonant O_2 and N_2, α_D is the absorption due to small water droplets (<50 μm) in clouds or haze, and α_R is the empirically determined extinction due to rain. Since scattering is not included in (2), α_R will introduce an additional error in the calculation of $T_B(\nu)$, particularly at high rain rates. However, such conditions will be anyway not suitable for atmospheric observations.

MPM calculates the complex refractivity thus allowing the calculation of the delay for a given model atmosphere as well. Furthermore, MPM is valid in the frequency range up to 1000 GHz for all conditions occurring in the troposphere where most of the absorption or emission will take place. Spectral stratospheric contributions of minor constituents and Zeeman-splitting have to be considered separately.

In order to calculate the radiances given by (2) the troposphere is divided in horizontal layers with a thickness of 100 m. For each layer, $\alpha(z, \nu)$ is calculated with a set of input parameters needed for MPM. Thus vertical profiles with an altitude resolution of 100 m of temperature $T(z)$, pressure $p(z)$, relative humidity $RH(z)$, droplet concentration $w(z)$, and point rain rate $R(z)$ are needed for the troposphere model.

The question arises how to define most economically the parameters of a probable vertical distribution of these input parameters. As described by *Robinson* [1988] the water vapor profile is better described in terms of relative humidity than water vapor density or partial pressure since the exponential decrease with altitude is removed. For example, in a cloud layer the relative humidity will be 100% and at ground level $RH(z_0)$ will be the surface value provided by a built-in meteorological instrument. At 10 km altitude where very little water vapor is present the relative humidity RH_{Top} is 0%. Furthermore, a tuning parameter for water vapor RH_{Ref} is introduced in such a manner that the relative humidity $RH(z)$ in the altitude range of 1.5 km above the observing site to 1.5 km above the top of the assumed cloud level (typically between 2 and 6 km) is equal to RH_{Ref}. The humidity profile is therefore represented by a three-piece linear function defined by interpolation between the endpoints $RH(z_0)$, RH_{Ref}, and RH_{Top} as this is illustrated in the upper right part of Figure 1.

The choice of the altitude range where $RH(z)$ is equal the tuning parameter is not critical for IWV and ILW retrieval and is therefore done intuitively. Moreover, it is evident that meteorological phenomena near the surface as low-level clouds, fog, or inversion layers cannot be adequately described by such a parameterization. Note that a dual-channel microwave measurement does not contain enough information in order to retrieve the real water vapor and liquid water profiles, but it allows the estimation of a probable distribution which can deviate substantially from the actual meteorological situation. However, the integrated quantities will only be little affected by the error in the profile assumption. The conversion to water vapor density or volume mixing ratio is done by using an empirical saturation pressure equation of water vapor given by *Bögel* [1977]. Integration of $\rho(z)$ over all layers yields to the IWV usually expressed in millimeters.

$$\mathrm{IWV} = 10^{-3}\int_{z_0}^{\infty} \rho(z)\, dz \tag{4}$$

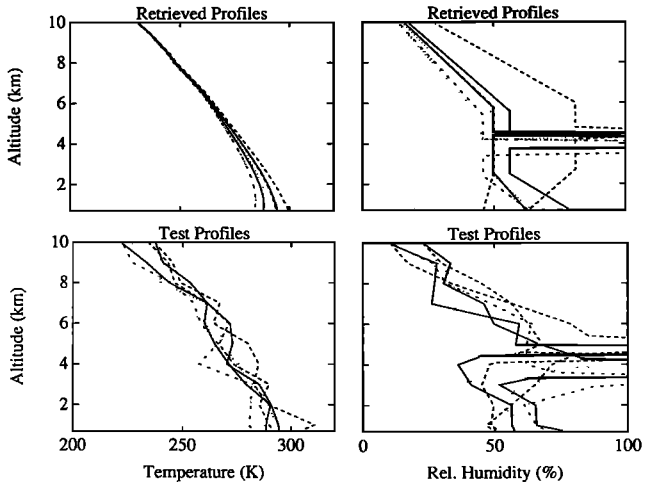

Fig. 1. Examples of randomly generated temperature and humidity test profiles for the error analysis and the corresponding profiles which are assumed by the profile retrieval algorithm. The different lines are due to the variation of the humidity profiles (e.g., RH_{Ref}) for cloudy conditions.

The pressure can be well described by a exponential decay with altitude using a measured surface value or a standard profile as in our case. For our purpose this estimation will have sufficient precision while, $T(z)$, which affects significantly the accuracy of the retrieved quantities, should be known as accurately as possible.

For $T(z)$ standard profiles (e.g., NASA Goddard Space Flight Center Monthly Mean Global Climatology [*Fleming et al.*, 1988]) interpolated for the corresponding latitude and season are used as initial profile. A better estimation of $T(z)$ will certainly be the monthly mean of radiosonde measurements from a meteorological station near the observing site. However, those are not always available. In order to take into account the high variability of the temperature, especially near the actual surface, an exponential fit of the initial profile to the surface value [*Robinson*, 1988] with a scale height of 3 km given by

$$T(z) = T_{\text{Init}}(z) + [T(z_0) - T_{\text{Init}}(z_0)]e^{-(z/H)} \tag{5}$$

is applied. The temperature matches therefore at ground level the surface value and approaches with increasing altitude the initial profile.

Clouds are modeled with a liquid water density profile $w(z)$ (g/m^3) and a relative humidity of 100%. The density $w(z)$ increases with altitude from the cloud base H_{Cloud} to the top of the cloud H_{Top} due to the decrease of the saturation pressure of water vapor with altitude. The difference between $\rho(z)$ in the cloud, and ρ_{Base} is the condensed water vapor of a rising air parcel, called the adiabatic liquid water content [*Rogers and Yau*, 1989]. Thus $w(z)$ in a cloud could be represented [*Slobin*, 1982] by

$$w(z) = (\rho_{\text{Base}} - \rho_{\text{Top}})\left(\frac{z - H_{\text{Cloud}}}{H_{\text{Top}} - H_{\text{Cloud}}}\right)C \tag{6}$$

where ρ_{Base} is the saturated water vapor density at the base of the cloud, ρ_{Top} is the saturated water vapor density at the top of the cloud, and C is the tuning factor due to different cloud types. Studies of the cloud structure [*Slobin*, 1982] showed that C is about half of the adiabatic liquid water content and depends on the cloud type. The entire cloud consists of several 100-m cloud layers at the adiabatic liquid water content (6) multiplied with the same tuning factor C. The top of the cloud H_{Top} is determined by the level where droplets begin to freeze out. Ice in clouds which occur above this level do not contribute significantly to microwave absorption and are neglected for our model. Thus only the liquid phase in the cloud can be detected. The temperature where ice crystal growth begins varies strongly depending on cloud type, ice nuclei concentration, and geographical location. It can be as low as −10°C or colder (supercooled clouds). Examination of different cloud types showed that they begin to freeze out at −3° and that 50% of the clouds containing ice crystals have a temperature at the top of the cloud of −10° [*Rogers and Yau*, 1989]. For simplicity and because it is very difficult to determine the actual H_{Top} due to the strong variation of ice formation, we took the altitude of the 0° level as H_{Top}. During winter when this altitude is near the surface due to the low temperatures, H_{Top} is chosen in a way that it is at least 2 km above ground level, which corresponds then to supercooled clouds. Low-level clouds are modeled by clouds at a higher altitudes as described above with the equivalent liquid water content.

The maximum liquid water density for heavy clouds is typically about 1 to 2 g/m^3. We imposed a maximum value of 1.25 g/m^3 on $w(z)$.

Finally, we have two parameters for the characterization of a cloud: The cloud base altitude H_{Cloud}, which implicitly means the cloud thickness, and the tuning parameter C (between 0.1 and 0.75) for the fine adjusting of the total liquid water content ILW.

Another source of liquid water is hygroscopic aerosols (w_A) occurring at relative humidities between 80% and 99.9%. They can contribute up to 0.1 g/m^3 to the liquid water density, particularly in smog conditions and for maritime climate. MPM includes an aerosol model for calculating the growth of droplets under haze conditions. The input parameters here are the aerosol concentration at 80% humidity, climate type, and relative humidity.

Rain is described by the rainrate profile $R(z)$ assuming a constant value from ground to the top of the cloud. The instantaneous suspended liquid water concentration $w_R(z)$ can be obtained by integrating over a standard dropsize distribution for a given point rain rate $R(z)$. For low rain rates w_R given in g/m^3 is approximately one tenth of the rain rate given in millimeters per hour. Note that with high rain rates scattering of waves at higher frequencies is not negligible any longer and may contribute significantly to errors in the IWV or ILW retrieval.

The total liquid water content ILW can be obtained by integrating $\rho_L(z)$ given by

$$\rho(z)_L = w(z) + w_A(z) + w_R(z) \tag{7}$$

in the same way as in (4).

With this definition of a simplified vertical structure of our model atmosphere the following parameters have to be changed during the iterative retrieval algorithm: The reference humidity RH_{Ref} determining the amount of water vapor, the cloud base altitude H_{Cloud} in steps of 100 m indicating the thickness of the layer containing water droplets and the ratio of the assumed droplet concentration to the

adiabatic value C allowing a continuous adjustment of the total amount of liquid water in combination with H_{Cloud}.

Since the sky emission of both channels depends on gaseous and liquid water, although with different sensitivities, each change of a parameter will influence the calculated T_B at 21 GHz (ν_1) and 31 GHz (ν_2) by different amounts. In order to adjust a parameter it should be known how a small change of RH_{Ref}, H_{Cloud}, and C would change $T_B(\nu_i)$ for a given observing situation. During the iteration, each variation of the parameters and $T_B(\nu_i)$ is recorded for the calculation of the sensitivity of brightness temperatures on parameter variation Q(parameter, ν_i), given by the ratio of $[T_{B,\text{Meas}} - T_B(\nu_i)]$ and the parameter difference. $T_B(\nu_1)$ will be dominated by the value of RH_{Ref} and therefore

$$RH_{\text{Ref}}^{i+1} = RH_{\text{Ref}}^{i} + \frac{T_B^i(\nu_1) - T_B^{i-1}(\nu_1)}{Q(RH_{\text{Ref}}, \nu_1)} \tag{8}$$

In a similar manner the other parameters for cloud liquid are derived from $T_B(\nu_2)$. In a first approach, RH_{Ref} is adjusted with (8) until $T_B(\nu_1)$ is equal to $T_{B,\text{Meas}}(\nu_1)$ within 2%. In a next step the cloud parameters are then tuned until the calculated and measured brightness temperatures $T_B(\nu_2)$ at 31 GHz do agree within 2%. Changing the cloud parameters results again in a new value for $T_B(\nu_1)$ which means that we have to proceed as in the first step. Several (typically 5–10) iterations are necessary until the exit criterion ($\Delta T_B < 2\%$) which is within the accuracy of the radiometer is fulfilled. Once a specific tropospheric condition is found where $T_{B,\text{Meas}}$ equals T_B other quantities such as sky brightness temperatures or zenith opacity for an arbitrary elevation and frequency up to 1000 GHz could be estimated using the capabilities of MPM. With the total tropospheric absorption along a slant path, obtained by integrating $\alpha(\nu, z)$ over all layers, the calculation of the absorption and emission of the troposphere can be used for the correction of stratospheric trace gas spectra where only the stratospheric emission is of interest.

A separation of the different contributions due to the liquid and vapor phases in the calculation of $\alpha(z, \nu)$ yields a set of coefficients for the linearized relations between IWV, ILW, and $T_B(\nu_i)$ or $\tau(\nu_i)$ as used by *Elgered et al.* [1982] and *Westwater and Guiraud* [1980]. Although our retrieval method has a higher complexity and needs more computation time, it is evident that more information with a better accuracy, particularly under cloudy conditions is obtainable than with a linear algorithm. Additionally, local climatology is only considered for the surface values of T, RH, and p and does not influence the retrieval performance as for the linear case.

3. Error Estimation of the Profile Algorithm

The overall error of IWV, ILW, $T_B(\nu)$, and $\tau(\nu)$ is primarily dependent on the error of the absorption model and the algorithm error including radiometer accuracy, deviation of the assumed profiles from the real profiles and the deviation T_B and $T_{B,\text{Meas}}$ due to the exit condition. We will treat first the intrinsic error of the algorithm.

The simplest way to quantify this error is a simulation of $T_{B,\text{Meas}}(\nu_i)$ with a few thousand known profiles of $T(z)$, $RH(z)$, and $w(z)$ for different seasons and climates.

TABLE 1. Yearly Averaged Mean Offset and rms Error (i.e., Deviation of the Retrieved Value From the Initial Value) of the Profile Retrieval Algorithm for a Mid-Latitude Site (500 Meters Above Sea Level)

Parameter	Mean Offset	rms
IWV	−0.15 mm	0.75 mm
ILW	0.0001 mm	0.036 mm
IWV*	−0.18 mm	0.43 mm
ILW*	0.004 mm	0.026 mm
$T_{B,90}$	−1.0 K	3.9 K
$T_{B,142}$	−1.7 K	5.9 K
$T_{B,204}$	−1.7 K	5.8 K
τ_{90}	−0.17 dB	0.65 dB
τ_{142}	−0.28 dB	1.14 dB
τ_{204}	−0.39 dB	1.74 dB

Brightness temperatures are taken in zenith direction in order to be not in the saturated region. The asterisks denote the error of the "Jungfraujoch" measurements (3580 meters above sea level) which are slighly different due to the high altutude.

Radiometric noise of 0.5 K rms is then added to the calculated $T_{B,\text{Meas}}(\nu_i)$ which are the input for the retrieval algorithm. The rms deviation of the retrieved IWV, ILW, $T_B(\nu)$, and $\tau(\nu)$ form the initial values will represent the algorithm error.

In order to have a wider variation of the initial profiles and to avoid site specific values as in radiosonde data bases a random generation of realistic profiles was favored. The IWV of the two thousand test profiles ranged from 5 to 80 mm with a mean IWV of 20 mm and the ILW varied from 0 to 1.2 mm with a mean value of 0.1 mm. Figure 1 shows an example of a set of generated and retrieved profiles and gives an impression how the algorithm estimates the temperature and water vapor profiles.

From the statistical analysis of two thousand test profiles for all seasons, yearly mean rms errors as listed in Table 1 or averaged absolute rms errors depending on the corresponding quantity (Figures 2, 3, and 4) are derived. The latter representation may be better in order to visualize the error for IWV, ILW, and opacity. The averaged absolute rms error of $T_B(\nu)$ decreases with increasing intensity above 150 K due to the saturation at about 300 K. The maximum rms deviations for $T_B(\nu)$ are 6, 8, and 8 K (≈5%–10%) for the

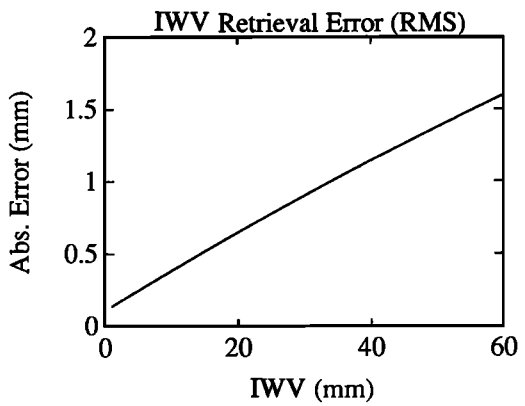

Fig. 2. Smoothed absolute rms error of the retrieval algorithm for the IWV, including profiling errors, radiometric noise of 0.5 K and exit criterion. The relative rms error is about 3%.

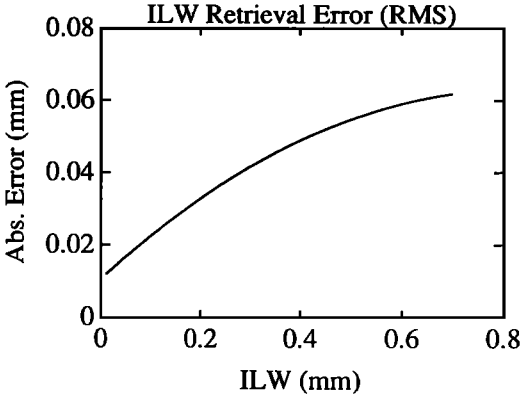

Fig. 3. Smoothed absolute rms error of the retrieval algorithm for the ILW, including profiling errors, radiometric noise of 0.5 K and exit criterion. For ILW values higher than 0.1 mm the relative rms error is between 10% and 20%, while at very low ILW values the rms error is always higher than 0.01 mm.

frequencies 90, 142, and 204 GHz, respectively. This maximum rms error occurs at about 150 K for all frequencies.

From the plots in Figures 2, 3, and 4 it can be seen that the rms error due to the profile variation and radiometer noise is about 3% for the IWV and between 10% and 20% for the ILW (ILW > 0.1 mm). The relative rms errors for the opacities are more or less the same for the considered frequencies and range from 25% for low opacities to 15% for higher opacities.

The error estimation has been done for low-elevation angles as well as zenith direction. Surprisingly, the zenith simulation showed slightly higher errors which are caused by the 0.5 K rms noise imposed on the lower calculated T_B at zenith. An estimation of the biasing of the IWV and ILW retrieval error due to absolute calibration errors of the radiometer has been carried out. For a radiometer elevation of 30° and a calibration error of 1 K (i.e., adding 1 K to T_B) at channel 1 (21.3 GHz) increases the IWV by about 0.5 mm and decreases the ILW by about 0.004 mm for a clear weather condition (IWV between 5 and 25 mm). An error of 1 K in channel 2 (31.5 GHz) yields a decrease of the IWV by about 0.2 mm and an increase of the ILW by about 0.013 mm. For zenith viewing instrument this error is nearly doubled due to lower air mass, i.e., lower T_B.

As listed in Table 1, biasing occurs also in the retrieval algorithm. Up to now we have neglected the error due to the absorption model MPM. This error can only be estimated by the comparison of calculations and field measurements for known meteorological conditions. However, $T(z)$ and $RH(z)$ are rarely known with sufficient accuracy. Even on-site launches of radiosondes exhibit an error which can be as high as the difference between different absorption models [*Westwater et al.*, 1990]. Furthermore, it is nearly impossible to obtain liquid water density profiles; thus the verification is restricted to clear weather situations.

Nevertheless, very useful information about absorption models can be gained by brightness temperature measurements and the corresponding retrieved value for T_B from the 21/31 GHz radiometer measurements. A study in the work by *Westwater et al.* [1990] showed that MPM [*Liebe*, 1989] predicts quite well brightness temperatures in the frequency ranges where nonresonant emission is dominant (e.g., 90 GHz), while at 21 and 31 GHz, MPM tends to underestimate the absorption (see also *Keihm* [1992]). However, the 1992 version of MPM exhibits higher absorption values than the 1989 version due to a slightly increased water vapor line intensity at 22.235 GHz and new coefficients for the 60-GHz oxygen complex [*Liebe et al.*, 1992] and might be therefore more accurate for water vapor retrieval algorithms. A comparison of both MPM versions yields a reduction of the retrieved IWV of about 4% when the 1992 version was used in the retrieval algorithm. Since MPM uses a lot of laboratory measurements performed at 138 GHz, the prediction at 142 and 204 GHz, which are in the window regions of the millimeter wave spectrum, are expected to be quite accurate.

An error in the absorption model may not result in a higher rms but will differ by a constant factor or by an offset from the true value (see also *Westwater et al.* [1990]). Therefore it will be difficult to give here an overall rms error for the retrieval of the considered quantities, but an upper limit for a bias error of the absorption model might be 5% (see also section 7).

Section 7 treats the verification of the predicted T_B by our own measurements at 142 and 204 GHz with two independent radiometers. In contrast to the comparison in the work by *Westwater et al.* [1990] we calculated $T_B(\nu)$ not from radiosonde measurements, but from 21/31 GHz measurements. Because the algorithm contains implicitly the absorption model, such a comparison is more regarded as a test of interfrequency predictability rather than the determination of absolute accuracy. However, if the predicted T_B do agree well with the corresponding measurements, it will show at least the consistency of the absorption model and justify its use for the determination of the opacity at other frequencies.

4. INSTRUMENTATION

Our instrument (Figure 5) consists of two triple-switched total power radiometers operating at 21.3 and 31.5 GHz. The bandwidths of the detectors are 100 MHz (SSB) and 200 MHz (DSB) for 21.3 and 31.5 GHz, respectively. During a measurement cycle the noise power is sequentially sampled from the temperature controlled hot load, cold load, and antenna position. A stability analysis for gain variations

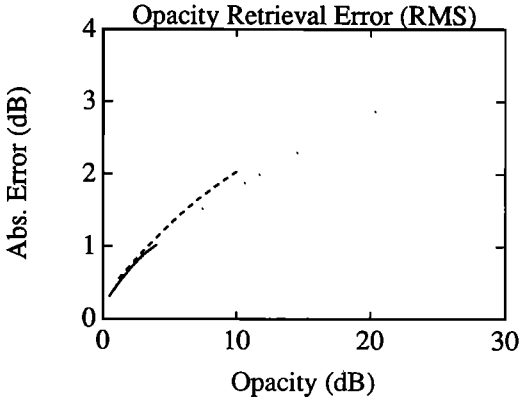

Fig. 4. Smoothed absolute rms error of the retrieval algorithm for the opacity, including profiling errors, radiometric noise of 0.5 K, and exit criterion. The opacity errors for the different frequencies 90 (solid line), 142 (dashed line), and 204 GHz (dotted line) are nearly the same.

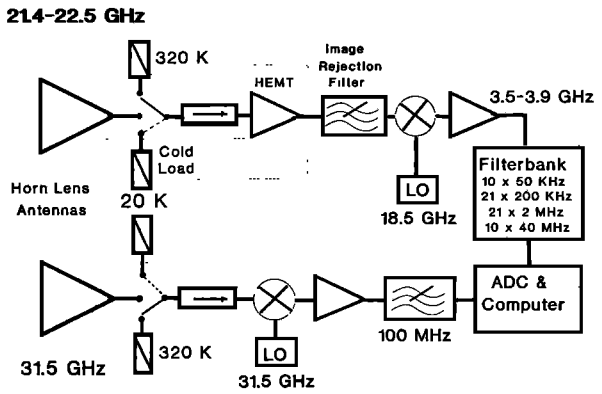

Fig. 5. Water vapor radiometer operating at 21.3, 22.2, and 31.5 GHz using a cooled (20 K) waveguide load for calibration.

showed that the cycle period should not be longer than a few seconds. On the other hand, during each switching, some time is waisted until the RC integrators reach a steady state, implying a long cycle period. Therefore the cycle period is set to 1 s. The integration time can be chosen in steps of the cycle periods. For our purposes it was enough to have a 15-min average which is the same integration time as of the other radiometers measuring the stratospheric trace gas spectra. However, for cloudy conditions with high sky brightness temperature variability shorter integration times would be more suitable.

In order to have a high absolute accuracy (<0.5 K), two waveguide loads at ambient temperatures of 310 and 20 K, respectively, are used as references. The advantage of this configuration is the use of a stable low temperature cold load which has a noise temperature close to the sky brightness temperature. The cold load is mounted inside an evacuated dewar on the cold head of a cryogenic cooling system. Since the small refrigerator unit of the closed helium cycle cooling system (separated compressor) can be mounted close to the waveguide switch inside the radiometer housing, continuous operational measurements are possible. Thin-wall stainless-steel waveguides inside the evacuated dewar reduce the heat transfer from the cold load to the warm environment. Between the dewar and the flange of a copper waveguide section to the switch, a Mylar foil separates the high-pressure area from the vacuum. Since losses of the waveguide sections increase the effective cold load noise temperature, the temperature of the line sections is also monitored for the calculation of the effective cold load noise temperature. In the next chapter the compensation of line losses and small temperature variations will be described. The single sideband 21 GHz receiver uses a high electron mobility transistor (HEMT) preamplifier for low-noise operation [*Peter et al.*, 1991]. This feature together with the phase-locked local oscillator and a filterbank should allow the measurement of the H_2O spectral line at 22.235 GHz from which the mesospheric water vapor distribution can be calculated [*Bevilacqua et al.*, 1989]. However, in this paper we will focus on tropospheric water vapor measurements which do not need spectrally resolved measurements at 22.235 GHz.

In order to observe the same air volume simultaneously, two high beam-efficiency horn-lens antennas with the same beamwidth of about 4.5° are used. Both radiometers are inside a weather resistant housing allowing measurements at different elevation angles. Thermal stabilization is achieved by mounting all microwave components on a heated aluminum plate, which has the same ambient temperature as the hot load.

The complete system consists of a small rack for the electronics, a PC with 12-bit analog-digital converters, a compressor for the cooling system, and a steerable front-end.

5. Calibration and Accuracy

Calibration is performed with two waveguide loads at 310 and 20 K ambient temperature, where their noise power and the corresponding output voltages characterize a linear relationship between antenna noise temperature and antenna output voltage, given by

$$T_{B,\mathrm{Ant}} = C(T_{\mathrm{Hot}} - T_{\mathrm{Cold}}) + T_{\mathrm{Hot}} \tag{9}$$

with C the ratio of the output voltages

$$C = \frac{V_{\mathrm{Ant}} - V_{\mathrm{Hot}}}{V_{\mathrm{Hot}} - V_{\mathrm{Cold}}} \tag{10}$$

The hot load is at the same temperature as all other components; thus self-emission of waveguide sections from the calibration source to the reference point after the first latching circulator (see Figure 5) are exactly compensated by their losses (i.e., T_{Hot} = 310 K).

For the cold load, which is the most important reference because its noise temperature is in the same range as the antenna temperature, self-emission due to losses has to be accounted for. A waveguide section with a linear temperature gradient and uniform loss along the line changes the effective noise power as follows [*Stelzenried*, 1968]:

$$T_{N,\mathrm{Eff}} = \left(1 - \frac{1 - \frac{1}{L}}{\ln(L)}\right) T_2 - \left(\frac{1}{L} - \frac{1 - \frac{1}{L}}{\ln(L)}\right) T_1 + \frac{T_N}{L} \tag{11}$$

where L is the loss factor, T_1 and T_2 are the input and output ambient temperatures of the waveguide section, and T_N is the input noise temperature (e.g., 20 K). If no temperature gradient is present, i.e., $T_1 = T_2$, (11) reduces to the well-known formula

$$T_{N,\mathrm{Eff}} = \left(1 - \frac{1}{L}\right) T + \frac{T_N}{L} \tag{12}$$

The effective cold load temperature T_{Cold} can now be calculated by using (11) or (12) for the different waveguide sections. However, direct measurements of the low attenuation of the waveguide components do not have sufficient accuracy, and they need to be adjusted by external calibration using an absorber immersed in liquid nitrogen and elevation scans (tipping curves).

The use of network analyzer measurements of the waveguide components and the knowledge of the temperatures along the line from the load to the reference point yields a first estimation of T_{Cold}, which is typically 55 and 85 K (±2 K) for the 21 and 31 GHz channel, respectively.

In a first step the antenna loss, which also increases $T_{B,\mathrm{Ant}}$ according to (12), is estimated by placing a styropor con-

tainer with an Ecosorb absorber immersed in liquid nitrogen (78 K) in front of the antenna. The antenna noise temperature assumes then the value of the physical absorber temperature which is determined by the boiling temperature of liquid nitrogen and the contribution of the styropor wall.

Small errors from the absorber calibration (≈1 K) can be corrected in a second step where the waveguide losses are adjusted by means of the "tipping curve" method. In a clear homogeneous troposphere the opacities are proportional to the air masses, which are dependent on the elevation angle. If the air mass is zero, there will be no absorption; i.e., $\tau = 0$. Extending the regression line of τ achieved at different elevation angles (i.e., different air masses) to zero, the effective cold load noise temperature characterized by the corresponding waveguide losses is determined. Linearization of the measured sky brightness temperatures with respect to τ or air mass is accomplished by the concept of linearized brightness temperatures T'_B [*Wu*, 1979]. The expression below gives the transformation from T_B to T'_B whose regression line should pass 2.64 K (cosmic background radiation T_{Bg}) at zero air mass:

$$T'_B = T_{Bg} - (T'_M - T_{Bg}) \ln\left(\frac{T_M - T_B}{T_M - T_{Bg}}\right) \qquad (13)$$

T_M and T'_M are highly correlated and correspond to the effective tropospheric temperature [see *Wu*, 1979] which may be approximated by 0.95 times the surface temperature. With relation (13) the radiometer is calibrated against the cosmic background radiation under the assumption of a stable atmosphere (no horizontal gradients). Therefore "tipping curves" are restricted to clear and dry weather conditions. For our purposes the "tipping curve" calibration is only used for the determination of the loss factors for the cold load correction. Once this has been done each variation of the reference loads due to temperature changes could be calculated with (11) and (12) which means that the calibration will be stable over long time periods no matter how the meteorological situations are. The overall accuracy is a combination of the uncertainty due to the precision (rms noise of the output voltages), the repeatability (unmodeled drifts and errors in the antenna brightness temperature calculation), and the calibration error from "tipping curve" measurements. Since it is difficult to evaluate every error source accurately, the best estimation of the overall accuracy might be the deviations of many different tipping curve measurements from the true value during a long period of observation. The tipping curve measurements made with our instrument indicate that the absolute accuracy is approximately 0.5 K.

6. Measurements in the Alpine Region

During a period of 6 months, from February to August 1991, measurements were carried out at the "Hochalpine Forschungsstation Jungfraujoch" (Switzerland) which is situated 3580 m above sea level. This station is primarily used by research groups requiring a dry unperturbed atmosphere. One purpose of our measurements was the confirmation of the tropospheric dryness above the station and another to prove operationality at an extremely dry atmosphere.

Observations were made at a low elevation angle of 20° in order to have sufficiently high brightness temperatures and

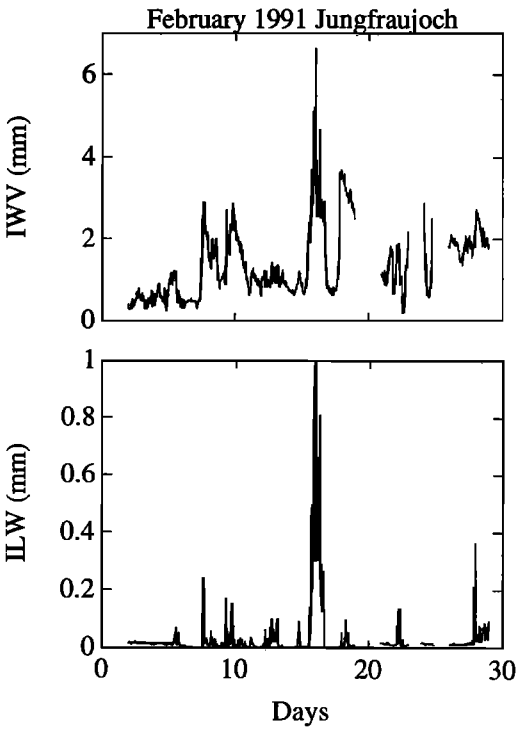

Fig. 6. Measured IWV and ILW above the "Jungfraujoch" research station (3580 meters above sea level) for February 1991. The high peaks around mid-February are probably not real but caused by water droplets and snow on the window during a stormy period.

therefore better absolute accuracy. On a clear and dry day, typical values of $T_{B,\mathrm{Meas}}$ were around 10 to 15 K. Application of our profile algorithm for water vapor (section 2) allows the retrieval of IWV and ILW. In Figures 6 and 7, examples of a very dry and a wet month are shown. Strongly varying IWV and high values of ILW indicate cloudy weather, which occurs more frequently in July due to cumulus cloud formation in the afternoon. The high peaks of IWV and ILW are probably not real because of the increased T_B due to the emission of water vapor droplets or snow on the polyethylene window during a storm. From these plots it can be seen that even in summer the IWV is quite low at this high-altitude station. A statistical analysis of the dryest (February) and the wettest (July) month are shown in Figure 8. In winter due to the low atmospheric temperature at this site the peak of the distribution, i.e., the value of the IWV, is in the range between 0 and 1 mm for nearly half of the observing time.

Indeed, the dryness of the troposphere is also confirmed by simultaneous measurements by a high-resolution IR Fourier transform spectrometer operated by a research group from the Solar Physics Laboratory, University of Liege (Belgium) [*Delbouille et al.*, 1989]. Figure 9 shows a scatterplot of the IWV measurements on several clear days at the same location. The mean IWV deviation of the IR measurements from the MW measurements is 0.09 mm (7%) and the rms deviation is 0.19 mm (16%). For the IWV retrieval with the IR instrument the vibration-rotation transition at 841.9 cm^{-1} was used. Some of the scatter might be explained by the different observing geometry. Our microwave radiometer had always the same observing direction,

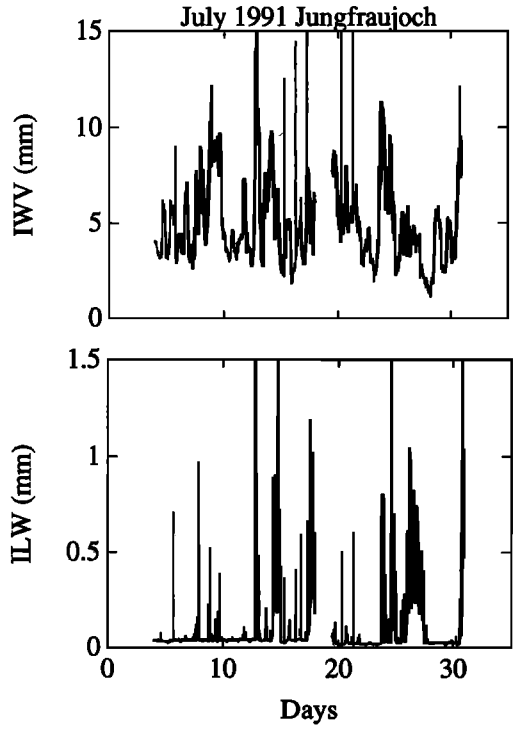

Fig. 7. "Jungfraujoch" measurements of IWV and ILW for July 1991. Typical are the periodically occurring peaks in liquid water due to cumulus cloud formation in the afternoon.

while the IR Fourier-transform spectrometer measured the path attenuation of the atmosphere between the Sun and the station (i.e., at different elevation angles due to the Sun movement).

Since in the profile algorithm for each brightness temperature measurement an appropriate model atmosphere is constructed, it is possible to estimate the zenith opacity at any other frequency, where MPM is valid (0–1000 GHz). This is an additional feature of our algorithm allowing attenuation statistics at another frequency, for example, 142 and 204 GHz for the correction of stratospheric trace gas spectra (O_3 and ClO, respectively). In the case of stratospheric emission this one has to be multiplied by a factor depending on tropospheric absorption as given below.

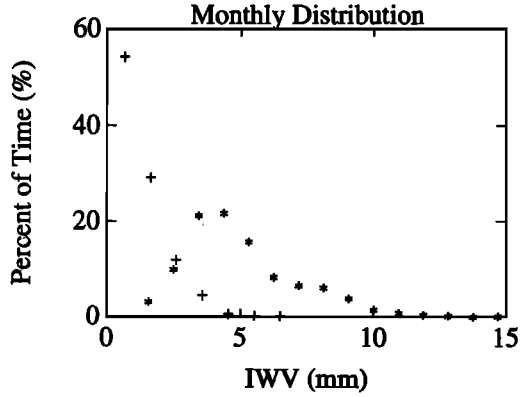

Fig. 8. Frequency distribution of water vapor above "Jungfraujoch" for the dryest (February) and wettest (July) month, indicated with a plus and an asterisk, respectively.

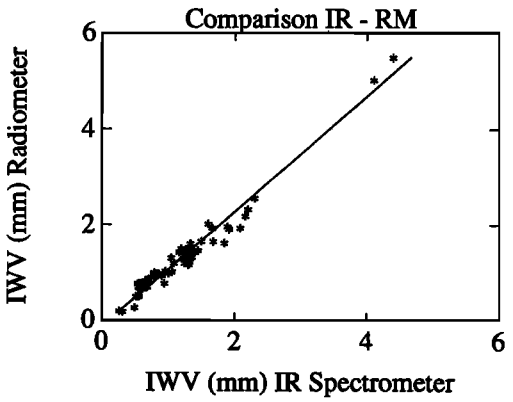

Fig. 9. Scatterplot of the IWV determined by IR spectroscopy (University of Liege) and our MW measurements at "Jungfraujoch." The rms difference is 0.20-mm IWV which corresponds to a deviation of about 16%.

$$T_{B,\mathrm{Strat}} = \left[T_{B,\mathrm{Meas}} - T_C e^{-\tau(\infty,\nu)} - \int_0^{z_T} T(z)\alpha(z,\nu) e^{-\tau(z,\nu)}\, dz \right] e^{\tau(z_T,\nu)} \qquad (14)$$

Here $\alpha(z, \nu)$ represents the total absorption (all molecules of the troposphere) and z_T is the height of the tropopause (≈15 km). In Figure 10, zenith opacities for the "Jungfraujoch" research station are calculated for a day in February 1991,

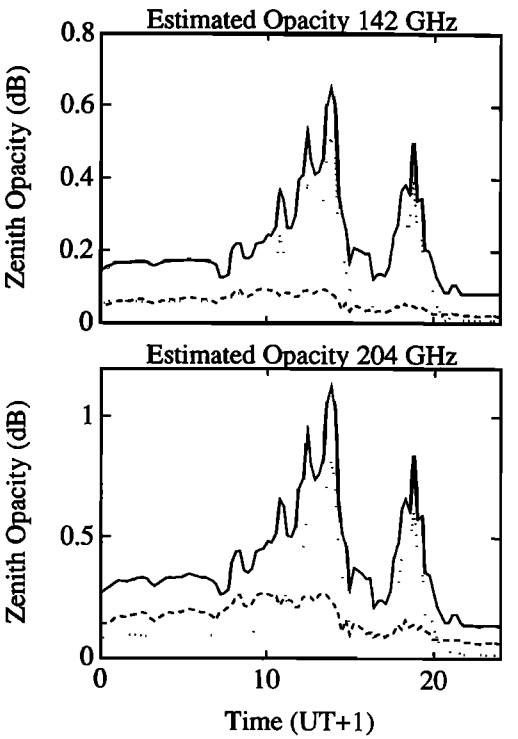

Fig. 10. Estimated zenith opacities at 142 and 204 GHz on the "Jungfraujoch" station for February 5, 1991. The contributions of liquid water (dotted line) and water vapor (dashed line) to the total zenith opacity (solid line) can be calculated separately.

TABLE 2. Calculated Mean Mass Absorption Coefficients κ and Mean Opacities for Dry Air τ_{Dry}

Frequency, GHz	Dry Air, τ_{Dry}	Vapor, κ_V	Liquid, κ_L
	Winter		
21	0.0280	0.0296	0.7464
31	0.0538	0.0058	1.3250
142	0.0437	0.0765	8.7581
204	0.0491	0.2173	14.0301
	Summer		
21	0.0263	0.0296	0.5098
31	0.0506	0.0059	1.0171
142	0.0394	0.0764	7.4310
204	0.0446	0.2108	11.1202

Coefficients κ are in decibels per millimeter of H_2O, and τ_{Dry} is in decibels. The upper section are the coefficients for February, and the values in the lower section indicate those for July at "Jungfraujoch" Station.

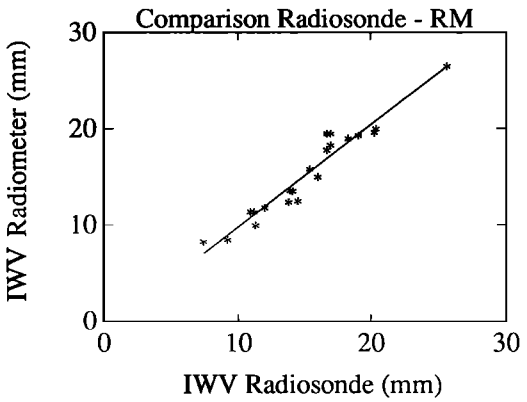

Fig. 11. Comparison of retrieved IWV with radiosonde measurements on few days during September, October, and November 1991. The rms difference is 1.1 mm which corresponds to a deviation of about 7%.

which correlates with the measurements given in Figures 6 and 7.

Separate calculation of the water vapor and liquid water absorption in the troposphere using the profile algorithm combined with MPM as this is illustrated in Figure 10 allows the determination of coefficients for the linear retrieval method for this site without the need of radiosonde data. The opacity τ for a frequency pair can be related linearly to IWV and ILW [*Westwater*, 1978] by

$$\tau_i = \tau_{Dry,i} + \kappa_{V,i}V + \kappa_{L,i}L \qquad (15)$$

where τ_{Dry} is the opacity due to dry air, κ_V and κ_L the path-averaged mass absorption coefficient of water vapor and liquid, respectively. Conversion of the opacity to linearized brightness temperatures (13) and solving (15) for V and L yields a set of coefficients for the linear retrieval algorithm as it is often used.

Table 2 shows the coefficients according to (15) for the "Jungfraujoch" Station for winter (February) and summer (July). The day-to-day variation of κ_V and κ_L is about 3–7%, while the variation of τ_{Dry} is less than 3%.

For comparison the mass absorption coefficients for Bern (560 masl), which is about 100 km away from the "Jungfraujoch" Station, are given in Table 3. They represent mean values deduced from our measurements during September 1991. The lower observing height $\tau_{Dry,i}$ is approximately 2 times higher than the corresponding values in Table 2. The coefficients for 21 and 31 GHz in Table 3 are very similar to those reported by *Westwater et al.* [1990] for Denver (Colorado). Note that both locations could be well compared since they are in mountain area. Similar estimations are also obtained by *Mätzler* [1992].

TABLE 3. Calculated Mean Mass Absorption Coefficients κ and Mean Opacities for Dry Air τ_{Dry}

Frequency, GHz	Dry Air, τ_{Dry}	Vapor, κ_V	Liquid, κ_L
21	0.0491	0.0250	0.4187
31	0.0950	0.0079	0.8627
142	0.0717	0.1049	7.3789
204	0.0809	0.2816	10.7501

Coefficients κ are in decibels per millimeter of H_2O, and τ_{Dry} is in decibels. The values are calculated from measurements during September 1991 at Bern.

Examination of the coefficients (particularly κ_L) for different months and sites reveals a drawback of the linear approach as given in (15): the time- and site-dependent variability of the retrieval coefficients.

7. Verification and Comparison With Radiometers Operating at 142 and 204 GHz

In order to estimate the performance of the profile retrieval algorithm and its prediction accuracy we made comparisons with an IR spectrometer (see chapter 6), radiosonde measurements and two independent radiometers operating at 142 and 204 GHz.

The radiosonde data under nonprecipitating conditions were taken from the national meteorological station Payerne (Switzerland), 30 km away from our observing site in Bern (47N, 7.5E, 560 meters above sea level). However, the humidity and temperature values in the lower layers might be different for the two sites. Therefore we made an exponential fit (scale height = 1 km) as given in (5) with our ground values of T and ρ. We reduced the effect of local differences of the IWV with this adjustment by typically 0.5–1 mm.

A statistical analysis of the retrieved IWV from water vapor radiometer data and radiosonde measurements on several days between September and October 1991 yields a mean deviation of 0.5 mm and a rms of 1.1 mm, which corresponds to rms deviation of about 7% of the mean IWV. Keeping in mind that the errors of the radiosonde measurements could be as high as this deviation, we can conclude that our observations did not significantly differ from the radiosonde measurements. The bias and the slope of the regression line in the scatterplot (Figure 11) is −0.7 mm and 1.01 mm, respectively, indicating a good behavior of our retrieval algorithm. Even in this coarse comparison (radiometer and radiosonde not at the same place) the retrieved IWV, the only quantity which can be compared to, is consistent with radiosonde data.

The interfrequency predictability of the algorithm was tested on nonprecipitating conditions with two other radiometers located at the same place. This comparison is not an

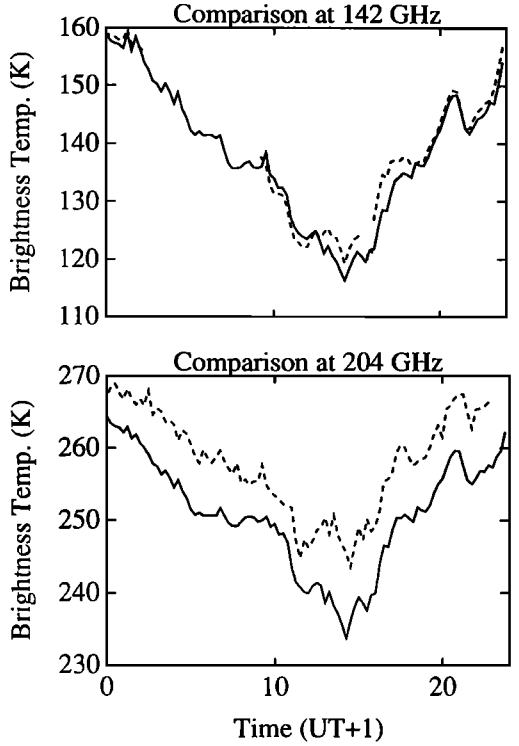

Fig. 12. Example of the comparison between independently measured brightness temperatures (dashed line) at 142 and 204 GHz, respectively, and estimated brightness temperatures (solid line) using the profile algorithm.

independent validation, since the retrieved model atmosphere contains implicitly the absorption model. However, the consistency between the different frequencies is a check of the absorption model and the retrieval algorithm.

The 142-GHz radiometer observed in the same direction as the water vapor radiometer at an elevation angle of 55°, while the 204-GHz radiometer had a lower elevation of 35°.

Figure 12 shows an example of the measurements made during September 1991 at Bern. The calculated brightness temperatures due to the assumed model atmosphere from the 21/31 GHz measurements reveal a good correlation with the measured brightness temperatures at 142 and 204 GHz. At certain days a nearly constant offset of the measured and estimated $T_B(\nu_i)$, particularly at 204 GHz, can reach values higher than 10 K. The stronger dependence on the assumed T and ρ profiles at 142 and 204 GHz and particularly the high sensitivity for ILW retrieval errors can certainly explain some of the observed discrepancy at those days. Another source of error is the absolute accuracy and stability of the 142- and 204-GHz radiometer of about 1 and 2 K, respectively, which can also contribute to such systematic deviations. It has to be kept in mind that a calibration error of the 21/31 GHz radiometer results also in a bias of the estimated T_B of approximately 3 times the brightness temperature error at 21 or 31 GHz.

The analysis of measured and estimated brightness temperatures on 20 days (≈1000 data points) during September and October 1991 yields a mean deviation (bias) of 0.3 and −1.6 K at 142 and 204 GHz, respectively. A negative value for the biases means that the retrieved T_B is lower than the measured one. Since the biases are within the T_B retrieval errors listed in Table 1 and the T_B errors of 1 and 2 K, respectively, resulting from the elevation angle uncertainty of 1° for the 142- and 204-GHz radiometer, the absorption model MPM (1992 version) together with the retrieval algorithm are consistent with independent measurements.

On the other hand, the rms deviation of 4.4 K (142 GHz) and 5.4 K (204 GHz) reveals rather the error due to (unknown) T and ρ profile variations than the absorption model error. Table 1 indicates that the rms deviations are lower than the retrieval error (rms) of T_B for various meteorological situations; i.e., they are within the error limits of the retrieval algorithm.

There is a strong evidence that the estimated accuracy of the absorption model of about 5% represents an upper limit for the MPM (1992) absorption coefficients. It is obvious that for a rigorous test of the absorption model simultaneous radiosonde and multifrequency measurements from exactly the same air volume are required as this has been done by *Westwater et al.* [1990].

8. Summary and Conclusions

For ground-based remote sensing applications the profile algorithm together with the millimeter wave absorption model MPM allows the estimation of path attenuation (or delay) for frequencies up to 1000 GHz as well as the total water vapor and liquid content in the troposphere. Although the profile retrieval algorithm is not as simple and elegant as the linear retrieval algorithm, it offers advantages over the linear approach.

The implicitly contained model atmosphere allows better adaption to the observing site without the use of radiosonde data bases which are mostly not available especially those with high accuracy. The only local information is surface temperature and humidity as well as standard temperature and pressure profiles for the corresponding latitude. Furthermore, no parameters for the retrieval have to be adapted to different seasons and meteorological conditions (e.g., high cloud liquid) as this is the case for the linear approach because the profile algorithm takes into account implicitly seasonal variation and nonlinearities generated by high cloud liquid.

It has been found that the retrieved quantities are consistent with brightness temperature measurements at 142 and 204 GHz. Independent confirmation was also obtained with an IR spectrometer (University of Liege, Belgium) and radiosonde data. The correction of ground-based millimeter wave observations with a profile algorithm using water vapor radiometer measurements and an absorption model is possible within the retrieval errors given in Table 1 and Figure 4.

For the explicit use in the tropospheric correction at 142 and 204 GHz (O_3 and ClO retrieval), the inclusion of a third frequency (e.g., 142 or 204 GHz) in the algorithm itself seems to be straightforward, but it will be difficult to find the appropriate determination of the atmospheric model parameters fulfilling the exit criterion at all frequencies simultaneously, particularly when the antennas do not observe the same air volume. Since both frequencies are located in the atmospheric window where emission due to liquid water is dominant and where they show a high correlation between each other, fine-tuning in order to get the agreement between measured and estimated T_B can be achieved by slightly changing the ILW, i.e., the 31-GHz emission.

Acknowledgments. The authors wish to thank the "Hochalpine Forschungsstation Jungfraujoch" for the opportunity to carry out our measurements. Special thanks are devoted to L. Delbouille and P. Demoulin (University of Liege, Belgium) for providing us with IWV measurements retrieved from high-resolution IR spectroscopic data. This work has been funded by Schweizerischer Nationalfonds NF contract 23330/12/13 and EVD-contract 1735.1.

REFERENCES

Bevilacqua, R. M., J. J. Olivero, and C. L. Croskey, Mesospheric water vapor measurements from Penn State: Monthly mean observations (1984–1987), *J. Geophys. Res.*, *94*, 12,807–12,818, 1989.

Bögel, W., Neue Näherungsgleichungen für den Sättigungsdruck des Wasserdampfes und für die in der Meteorologie gebräuchlichen Luftfeuchte-Parameter, *Rep. DLR-FB 77-52*, Dtsch. Forsch. und Vers. für Luft- und Raumfahrt, Oberpfaffenhofen, Germany, 1977.

De Amici, G., M. Bersanelli, A. Kogut, S. Levin, M. Limon, and G. F. Smoot, The temperature of the cosmic microwave background radiation at 3.8 GHz: Results of a measurements from the South Pole site, *Astrophys. J.*, *381*, 341–347, 1991.

Delbouille, L., G. Roland, J. Blavier, and R. Zander, The Jungfraujoch Station as part of the European ground based observations network, paper presented at 28th Liege International Astrophysics Colloquium—Our Changing Atmosphere, Inst. d'Astrophys. Univ. de Liege, Cointe-Ougree, Belgium, June 26–30, 1989.

Elgered, G., B. O. Rönnäng, and J. I. H. Askne, Measurement of atmospheric water vapor with microwave radiometry, *Radio Sci.*, *17*, 1258–1264, 1982.

Elgered, G., B. O. Rönnäng, E. Winberg, and J. I. H. Askne, Satellite-Earth range measurements: Correction of the excess path length due to atmospheric water vapour by ground based microwave radiometry, *ESA Res. Rep. 147*, Eur. Space Agency, Neuilly, France, April 1985.

Fleming, E. L., S. Chandra, M. R. Schoeberl, and J. J. Barnett, Monthly mean global climatology of temperature, wind, geopotential height and pressure for 0–120 km, *NASA Tech. Memo.*, *NASA TM-100697*, 1988.

Gerber, L., and N. Kämpfer, High resolution multi-channel mm-wave radiometer for the detection of stratospheric ClO, *Proc. SPIE Int. Soc. Opt. Eng.*, *1991*, 211–217, 1991.

Guiraud, F. O., J. Howard, and D. C. Hogg, A dual-channel microwave radiometer for measurement of precipitable water vapor and liquid, *IEEE Trans. Geosci. Electron.*, *GE-17*, 129–136, 1979.

Hogg, D. C., F. O. Guiraud, J. B. Snider, M. T. Decker, and E. R. Westwater, A steerable dual-channel microwave radiometer for measurement of water vapor and liquid in the troposphere, *J. Appl. Meteorol.*, *22*, 789–806, 1983.

Kämpfer, N., P. Bodenmann, and R. Peter, Ground-based microwave radiometry of ozone, *Proc. SPIE Int. Soc. Opt. Eng.*, *1991*, 314–322, 1991.

Keihm, S. J., Atmospheric absorption from 20–32 GHz: Radiometric constraints on the vapor and oxygen components, paper presented at Specialist Meeting on Microwave Radiometry and Remote Sensing $\mu\lambda$Rad 92, U.S. Dep. of Comm. Natl. Oceanic and Atmos. Admin., Boulder, Colo., Jan. 1992.

Liebe, H. J., An updated model for millimeter wave propagation in moist air, *Radio Sci.*, *20*, 1069–1089, 1985.

Liebe, H. J., MPM—An atmospheric millimeter-wave propagation model, *Int. J. Infrared Millimeter Waves*, *10*, 631–650, 1989.

Liebe, H. J., G. A. Hufford, and T. Manabe, A model for the complex permittivity of water at frequencies below 1 THz, *Int. J. Infrared Millimeter Waves*, *12*, 659–675, 1991.

Liebe, H. J., P. W. Rosenkranz, and G. A. Hufford, Atmospheric 60 GHz oxygen spectrum: New laboratory measurements and line parameters, *J. Quant. Spectrosc. Radiat. Transfer*, in press, 1992.

Mätzler, Ch., Ground-based observations of atmospheric radiation at five frequencies between 4.9 and 94 GHz, *Radio Science*, *27*, 403–415, 1992.

Peter, R., and N. Kampfer, Estimation of tropospheric opacity with a 20/30 GHz radiometer for the correction of ground based mm-wave measurements of stratospheric trace gases, paper presented at IGARSS 91, Espoo, Finland, June 1991.

Peter, R., M. V. Schneider, and Y. S. Wu, High-performance HEMT amplifiers with a simple low-loss matching network, *IEEE Trans. Microwave Theory Tech.*, *39*, 1673–1675, 1991.

Robinson, S. E., The profile algorithm for microwave delay estimation from water vapor radiometer data, *Radio Sci.*, *23*, 401–408, 1988.

Rogers, R. R., and M. K. Yau, *A short course in cloud physics*, *Int. Ser. Natl. Philos.*, vol. 113, Pergamon, New York, 1989.

Slobin, S. D., Microwave noise temperature and attenuation of clouds: Statistics of these effects at various sites in the United States, Alaska and Hawaii, *Radio Sci.*, *17*, 1443–1454, 1982.

Stelzenried, C. T., Microwave thermal noise standards, *IEEE Trans. Microwave Theory Tech.*, *MTT-16*, 664–655, 1968.

Ulaby, F. T., R. K. Moore, and A. K. Fung, *Microwave Remote Sensing: Active and Passive*, vol. 1, *Microwave Remote Sensing Fundamentals and Radiometry*, Addison-Wessley, Reading, Mass., 1981.

Waters, J. W., Absorption and emission by atmospheric gases, in *Methods of Experimental Physics: Astrophysics*, vol. 12, part B, edited by M. L. Meeks, pp. 142–175, Academic, San Diego, Calif., 1976.

Westwater, E. R., The accuracy of water vapor and cloud liquid determination by dual-frequency ground based microwave radiometry, *Radio Sci.*, *13*, 677–685, 1978.

Westwater, E. R., and F. O. Guiraud, Ground-based microwave radiometric retrieval of precipitable water vapor in the presence of clouds with high liquid content, *Radio Sci.*, *15*, 947–957, 1980.

Westwater, E. R., J. B. Snider, and M. J. Falls, Ground-based radiometric observations of atmospheric emission and attenuation at 20.6, 31.65, and 90 GHz: A comparison of measurements and theory, *IEEE Trans. Antennas Propag.*, *38*, 1569–1579, 1990.

Wu, S.-C., Optimum frequencies of passive microwave radiometer for tropospheric path length correction, *IEEE Trans. Antennas Propag.*, *AP-27*, 233–239, 1979.

N. Kämpfer and R. Peter, University of Berne, Institute of Applied Physics, Sidlerstrasse 5, 3012 Berne, Switzerland.

(Received March 30, 1992;
revised July 10, 1992;
accepted July 13, 1992.)